Seasonal variations in rain cells propagation over Central Africa and association with diurnal rainfall regimes.

Pierre Camberlin, Vincent Moron, Nathalie Philippon, François Xavier Mengouna, Derbetini A. Vondou

Received: 13 November 2023 | Revised: 3 April 2024 | Accepted: 8 April 2024

DOI: 10.1002/joc.8466

RESEARCH ARTICLE

International Journal of Climatology RMetS

Seasonal variations in rain cells propagation over Central Africa and association with diurnal rainfall regimes

Pierre Camberlin[1] | **Vincent Moron**[2,3] | **Nathalie Philippon**[4] | **François Xavier Mengouna**[5] | **Derbetini A. Vondou**[5]

[1]Biogéosciences/CRC, Université de Bourgogne/CNRS, Dijon, France

[2]Aix-Marseille University, CNRS, IRD, INRAE, Collège de France CEREGE, Aix-en-Provence, France

[3]International Research Institute for Climate and Society, Lamont-Doherty Earth Observatory, Columbia University, Palisades, New York, USA

[4]Institut des Géosciences de l'Environnement, UGA, CNRS, IRD, Grenoble INP, Grenoble, France

[5]Laboratory for Environmental Modelling and Atmospheric Physics (LEMAP), Department of Physics, Faculty of Science, University of Yaounde 1, Yaounde, Cameroon

Correspondence
Pierre Camberlin, Biogéosciences/CRC, Université de Bourgogne/CNRS, Dijon, France.
Email: pierre.camberlin@u-bourgogne.fr

Funding information
Institut national des sciences de l'Univers; Centre National d'Etudes Spatiales

Abstract

Three-hourly data from two satellite rainfall estimates products, PERSIANN and TMPA, are analysed to document the seasonal patterns of diurnal rainfall distribution over the Congo Basin and neighbouring areas. PERSIANN data for 2001–2017, at a one-hour time-scale, are further used to identify rain cells ($\geq$4 mm·h^{-1}) in an attempt to explain the diurnal rainfall variations. Over land areas, an afternoon rainfall maximum is clearly shown, but over much of the region only a minor part of the rains (20%–30%) falls in the wettest 3-h period. Substantial rains (often 50%–60%) occur in the evening and at night, as a progressively delayed peak from east to west, but a seasonal change is found in the meridional propagation of the peak diurnal rainfall, in a south-westerly direction in January, and a north-westerly direction in July. Rain cells have prominent genesis areas west of high terrain, but can develop over most regions, with a peak genesis time slightly ahead the diurnal phase of the rains. The size, mean lifetime and mean rainfall intensity of the rain cells are strongly related to each other and display a semi-annual cycle not fully in phase with the seasonal cycle of the rains. The mean rain cell propagation speed (6.7 m·s^{-1}) is much lower than in previous studies, which focused on mesoscale convective systems. Rain cells which have a longer lifetime move much faster, the mean speed of those lasting less than 6 h being half that of those lasting at least 24 h. Most (86%) of the mobile rain cells propagate westward, but the meridional component of their propagation shows an annual cycle (southward in austral summer, northward in boreal summer) which matches the mid-tropospheric winds and explains the seasonal changes in the diurnal rainfall peak.

KEYWORDS

Central Africa, diurnal cycle, rain cells, rainfall, rainfall systems propagation, seasonal variations

1 | INTRODUCTION

Central Africa has been off the radar of climatological research for many years, and the mechanisms of rainfall variability in the region are still poorly understood (Dezfuli, 2017; Nicholson, 2022). While significant advances have been made in the description and understanding of West African rainfall disturbances (Lafore et al., 2011; Parker & Diop-Kane, 2017), much less is known about those of Central Africa (Pokam Mba et al., 2022). Early studies were carried out by French tropical meteorologists in the 1950s, based on synoptic and upper-air observations. Tschirhart (1959) identified four types of atmospheric disturbances: (1) squall lines, shifting westward in connection with mid-tropospheric winds; (2) quasi-stationary zonal disturbances, mostly associated with the northern limit of the southwesterly 'monsoon' flow; (3) cyclonic convergence disturbances, isolated, in a strongly meridional flow from the northeast or the southeast and (4) maritime disturbances, mostly at night in a northwesterly flow from the Gulf of Guinea. Jeandidier and Rainteau (1957) and Tschirhart (1959) found that strong convective systems develop along the convergence line between the monsoon and the easterlies, called Congo Air Boundary (CAB, or 'Front Equatorial Africain' in their terminology), especially when the CAB shifts eastward. The CAB recently attracted renewed interest to explain southern Africa rainfall variability (Howard & Washington, 2019).

With satellite observations, our knowledge on Central Africa rainfall disturbances improved. Jackson et al. (2009) studied the frequency of mesoscale convective systems (MCSs, defined as precipitation patches with at least 2000 km^2 with temperature below 250 K, and 185 km^2 below 225 K). The statistics were relative only, because of the low sampling frequency and narrow swath of the satellite radar, and the MCSs propagation was not examined. The MCSs seasonal cycle follows that of rainfall, but the two main rainy periods of March–May (MAM) and September–November (SON) are not symmetrical, with more MCSs in SON and along a northeast-southwest line across the region, while the distribution is more zonal in MAM.

Laing et al. (2011) analysed the timing, duration and frequency of westward-propagating MCSs over Equatorial Africa. These systems have an average 17.6-h duration and 673-km span. Most have zonal phase speeds of 8–16 $m{\cdot}s^{-1}$. Some long-lasting systems result from the regeneration of convection through multiple diurnal cycles while propagating westward, but the duration of convective systems is generally smaller than in northern tropical Africa. These equatorial westward-moving disturbances are modulated by eastward-moving Kelvin waves (Laing et al., 2011; Nguyen & Duvel, 2008).

Recent studies documented significant changes in convective disturbances in the last decades. Raghavendra et al. (2018) found increases in the extent (number of pixels with low brightness temperature) and intensity (cloud top temperatures) of thunderstorms over the Congo Basin during the April–June season between 1982 and 2016. Taylor et al. (2018) studied monthly trends in the frequency of intense MCSs over Equatorial Africa (15° W–28° E), and similarly found more MCSs in February and April from 1999 onward. None of these two studies analysed the characteristics of individual storms.

Hartman (2021) produced a 33-year MCS climatology for the MAM and SON rainy seasons from infrared satellite data (GridSat-B1). Convective clusters were selected based on a −48°C cloud top temperature threshold and an area of over 10,000 km^2, for three successive 3-hourly observations. He found MCS activity hot spots over Lake Victoria, mountain ranges close to the western Rift Valley near 28–33° E, and near coastal Cameroon. The western Rift hot spot is associated with a 650 hPa vorticity couplet. MCS initiation is greatest in the afternoon, but maximum intensities are at night. MCSs generally move westward at more than 9 $m{\cdot}s^{-1}$ over land areas. In both seasons, patterns of MCSs displacement match spatially the 650 hPa fields of average wind and vertical shear. Andrews et al. (2024) analysed the MCSs contribution to total rainfall over the Congo Basin using 20 years of IMERG precipitation estimates. A 80% contribution was found over the continental interior throughout the year. Baidu et al. (2022) noted some relationships with vertical wind shear, whose strength affects various parameters of the MCS such as their speed, size, rain-rate and lifetime.

The present study re-investigates the behaviour of rain cells (defined as any individual wet grid-point and contiguous wet patches of rainfall occurrence, i.e., not only MCSs) over Central Africa. It relies on precipitation estimates, instead of convection proxies (such as brightness temperature), used in most other studies to detect cold clouds. This enables us to derive information on the rainfall intensity of rain cells and to relate it to other characteristics such as the lifetime and size of the cells. Except for Laing et al. (2008) and Hartman (2021), previous studies on convective systems in Central Africa focused on their zonal propagation, as most of them clearly move westward. In this study, we also have a close look at the meridional component of the propagations and its seasonal variations. It is hypothesized that these are important characteristics of the rain cells propagation.

Another objective is to use this information on rain cells to explain the patterns of diurnal rainfall distribution over Central Africa. It is expected that these diurnal regimes strongly depend on the development and propagation of rain cells. Many parts of Central Africa are

characterized by a dominant late afternoon rainfall maximum (Dezfuli, 2017; Vondou et al., 2017), related to daytime convection and to MCSs occurrence (Andrews et al., 2024; Jackson et al., 2009). The diurnal cycle of MCSs shows maximum frequency around 15:00–21:00 LST, but there is substantial MCS activity at night, during which volumetric rain per MCS increases. Deviations to the overall afternoon peak also occur. For instance, over the Bight of Bonny off the coast of Cameroon, the maximum is at noon or in the morning (Vondou et al., 2010). At the eastern extremity of the region, the larger Rift Valley lakes (Tanganyika, Albert) display a late night to early morning maximum (Camberlin et al., 2018), attributed to local convergence associated with land breezes. In the central Congo Basin, Samba-Kimbata (1988), based on observations at 9 stations, noted a large share of the rains starting in the second half of the night (35% and 32% between 00:00 and 06:00 at Kindu and Boende, respectively, in the Democratic Republic of Congo [DRC]). These nighttime rains are still not well understood. Andrews et al. (2024) found that MCS rainfall shows a unimodal diurnal cycle in the equinoctial seasons (peak at 16:00/17:00 LST and minimum at 05:00/06:00 LST) but inhomogeneous patterns in the solsticial seasons. Late night hours display a slightly higher contribution of MCSs to total rainfall.

Despite the recent advances, there is still an imperfect understanding of the spatial distribution of the diurnal peak rainfall and its seasonal variations. The present article, therefore, seeks to explain these patterns by considering rain cells movements and what drives them. Liu (2011) showed that analysing the combinations of life cycles of various precipitation systems helps to interpret the diurnal cycles of tropical rainfall. Additionally, analysing rain cells characteristics is key to a better appraisal of forthcoming changes in rainfall intensity due to global warming (Lochbihler et al., 2017). Section 2 presents the data, Section 3 the methods and Section 4 the results, starting from the spatial patterns of mean diurnal rainfall distribution, then the characteristics of rain cells, and finally the relationship between wind flows and rain cells motion.

2 | DATA

2.1 | Satellite rainfall estimates

The study is based on two gridded rainfall data sets, merging satellite estimates and rain gauge observations, both at a 0.25° latitude x longitude resolution. Data were extracted over a region covering Central Africa from the Atlantic Ocean to the Western Rift Valley (9–31° E, 7° S–7° N). This includes most of the Congo River Basin, whose central part ('Cuvette Centrale') is characterized by flat, low-elevation terrain (Figure 1). Discontinuous mountain ranges and ridges of moderate elevation are found on all sides of the region (Chaillu Mountains and Bateke Plateaux to the west, Kasai upper reaches to the south, Nile-Congo-Chad watersheds to the north). Only in the east is found a continuous line of higher elevation mountain ranges (often above 1500 m), in a north–south direction, related to the Western Rift Valley.

The first gridded data set is TMPA (Tropical Rainfall Measuring Mission Multi-satellite Precipitation Analysis) 3B42 which combines precipitation radar, microwave measurements and polar-orbiting and geostationary satellite images to obtain 3-hourly rainfall estimates, scaled to match the GPCP (Global Precipitation Climatology Project) monthly rain gauge analyses (Huffman et al., 2007). We made use of version 7 over the years 1998–2014.

The second dataset, PERSIANN (Precipitation Estimation from Remotely Sensed Information using Artificial Neural Networks; Hong et al., 2004; Nguyen et al., 2019) is initially available at an hourly resolution, and used for rain-cell tracking over the period 2001–2017. Estimates are based on infrared brightness temperature images provided by geostationary satellites. Compared to Hartman (2021), we considered hourly instead of 3-hourly data to track the rain cells. Since we target both small and large size convective systems, a high resolution timescale was needed for adequate tracking. We also made use of a 3-hourly version of PERSIANN to analyse the diurnal cycle of rainfall as a comparison with TMPA.

TMPA and PERSIANN data were compared with rain gauge observations across Central Africa at monthly and daily timescales (Camberlin, Barraud, et al., 2019). For daily rainfall amounts, TMPA showed the best skills among the seven products tested (ARC, CHIRPS, CMORPH, PERSIANN, TAPEER, TARCAT, TMPA), while PERSIANN had lower correlation coefficients but the second lowest root-mean-square error after TMPA when tested against fully independent stations.

At sub-daily timescales, these products were additionally subject to two rudimentary skill assessments. Firstly, due to the paucity of recent in situ rainfall data, old (1951–1980) 3-h long-term mean rainfall occurrence data from nine stations (Berberati, Bangui and Bangassou in the CAR, Ouesso and Impfondo in Congo-Brazzaville, Mbandaka, Boende, Kisangani and Kindu in the DRC) were extracted from the climatology of Samba-Kimbata (1988). In addition to the differences in the periods, the evaluation is slightly biased by the fact that in the observation, rainfall occurrence was allocated to the first 3-h period of the rain event, even if it lasted more than 3 h, whereas in the satellite estimates the rain falling during each 3-h bin was a separate occurrence. Despite these shortcomings, the mean 3-hourly distribution agrees

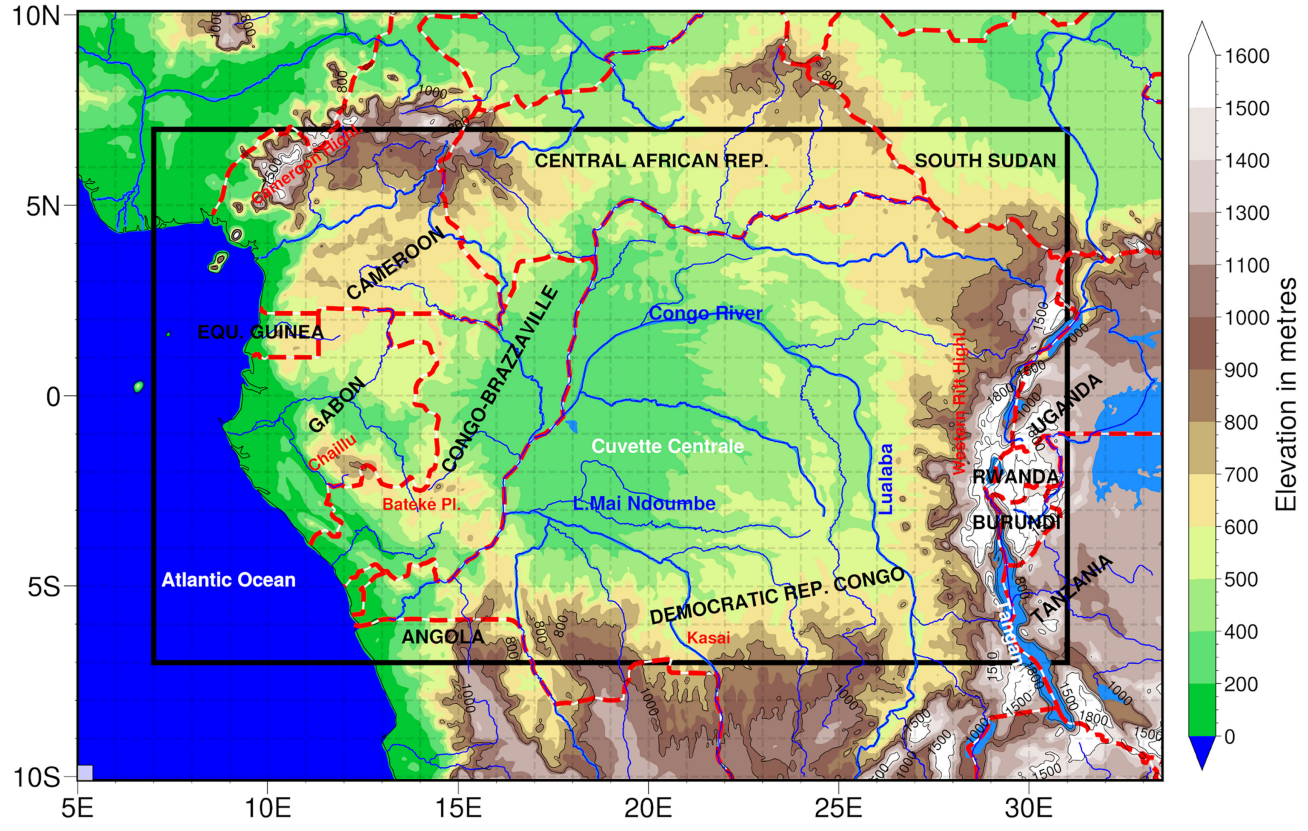

FIGURE 1 Location and elevation map of Central Africa.

reasonably well between the observations and the TMPA estimates ($r = 0.55$ for $N = 72$ across all stations). This is less so for PERSIANN ($r = 0.37$), mainly because this product tends to slightly exaggerate the afternoon maximum, though the agreement is good at the northern and western locations.

Secondly, 1-h PERSIANN rainfall amounts from 2015 to 2017 were validated at 5 automatic weather stations located in eastern DRC and Congo-Brazzaville (Camberlin, Barraud, et al., 2019). Correlations ($N = 11{,}577$–16,900 hourly records) are moderate, due to the spatial scale mismatch, but clearly peak at 0-h lag at 4 out of 5 stations, with highly significant values ($p < 0.001$). The mean diurnal cycle, showing an early to late afternoon maximum, is also correctly reproduced at 4 out of 5 stations. In conclusion, although this sub-daily skill assessment remains basic, a fair confidence can be put in the hourly and 3-hourly satellite estimates used in the study.

2.2 | Other data

Reanalysis data from ERA5 (European Centre for Medium-Range Weather Forecasts 5th Re-Analysis; C3S, 2017) were used to document the wind patterns. Twenty-two vertical levels were retained from 1000 to 200 hPa, at 0.25° horizontal resolution. ERA5 was shown to better reproduce climate fields than previous reanalysis data over Africa (Gleixner et al., 2020).

3 | METHODS

3.1 | Mean diurnal cycle

The mean diurnal cycle of the rains is described by two simple indicators. First, the percentage rainfall occurring in the mean wettest 3-h period (W3) is the metric used to depict the amplitude of the diurnal cycle. Second, the timing of the mean wettest 3-h period describes the phase of the diurnal cycle. Both indicators are mapped on a monthly basis. Sample time-longitude cross-sections are also plotted. All times given are UTC, which is from about half an hour to two hours behind Central Africa local solar time (LST) depending on the longitude (i.e., LST is UTC + 0.5 to UTC + 2). Note that in the following the 00:00 precipitation designates precipitation falling within the 00:00 to 02:59 time-slot.

3.2 | Tracking of rain cells

Following Sauvageot et al. (1999) and Capsoni et al. (2008), the term 'rain cell' is retained to designate a

group of connected rain-bearing pixels (in a gridded rainfall data set) whose rain-rate value exceeds a given threshold. In this study, rain cells are defined from PERSIANN hourly data as ensembles of contiguous 0.25° pixels, all recording at least 4 mm per hour. This threshold has been retained to document only the intense rain systems, and through a visual examination of the tracking algorithm performance using different thresholds between 2 and 5 mm. Hourly precipitation above 4 mm represents only 17% of the hourly-pixel rain observations but contributes to 52% of the total rainfall amount averaged over the study area. Fu et al. (2020) found that Central Africa was among the tropical regions with the greatest share of high intensity (above 4 $mm \cdot h^{-1}$) rain cells.

No minimum size and no minimum duration are required for the rain cells selection (hence, the study does not target MCSs specifically). The tracking algorithm of rain cells derives from Moron and Robertson (2021). For a given cell to be tracked to the next image, there must be a spatial contiguity/overlap of at least one grid-square between two successive images. Each rain cell history is then defined by the following attributes: its lifetime (in h), the geographical location of the centre of gravity of the cell at its origin (XY1) and at its dissipation (XY2), the average propagation speed between XY1 and XY2, the time and date of its origin and dissipation, the maximum size of the cell during its lifetime, and the mean precipitation intensity.

The algorithm allows for rain cells merging and splitting. When merging, only the parent cell with the longest lifetime is retained. When splitting, only the child cell with the longest lifetime is retained. In some occasions, the merging or splitting abruptly changes the centre of gravity, therefore artificially increasing the propagation speed, but this has a minor impact on the final statistics. Similarly, statistics on lifetimes do not account for systems that may exit the region. Central Africa being mostly a region of origin of rain cells, the reciprocal (a rain cell originating from outside the region) is a rare occurrence. However, the rain cells initiated within 1° of the outer limits of the domain, whose extent and lifetime are possibly underestimated, are excluded to avoid biases in rain cells statistics.

In order to examine the role of the winds in the rain cells' displacement, the motion vector of each cell is defined between the origin (XY1) and dissipation (XY2) by its zonal and meridional components. These are compared to the zonal and meridional components of the wind at different levels, as well as to the vertical wind shear. The comparison is carried out first on monthly means, then for individual rain cells (in this case the wind flow is that observed on the day of the rain cell, i.e., in the middle of the cell's lifetime, and at the cell's centre of gravity). The angle between the motion vector and the wind vector is also computed.

4 | RESULTS

4.1 | Spatial patterns of mean diurnal rainfall distribution

Maps of the diurnal rainfall distribution in TMPA and PERSIANN are presented for months representative of the four seasons found over the region. January (July) maps correspond to the time when the rainbelt is furthest south (north) and drier conditions develop in the north (south). April and October correspond to the boreal spring and autumn rainy seasons.

The percentage of rainfall occurring during the wettest 3-h period on average (W3, Figure 2) shows that the diurnal cycle is not highly pronounced over many areas. In particular, in the central part of the Congo Basin, W3 rarely exceeds 20%–25%. By contrast, some areas show stronger diurnal variations, with about 30%–45% of precipitation in the wettest 3-h timeslot. They are located (i) immediately west of mountain ranges (e.g., Western Rift Highlands near 28–30° E, Cameroon Highlands, Chaillu Massif in Gabon, cf. Figure 1) and (ii) near the northern and southern margins of the rainbelt (especially in January and July, respectively). TMPA and PERSIANN agree well on these patterns. A larger diurnal amplitude was also found in the Cameroon Highlands by Vondou et al. (2010). It is hypothesized that higher ground enhances daytime convection, resulting in a greater diurnal concentration of the rains. Similarly, atmospheric conditions in the rainbelt margins (e.g., 3–5° N in January) are not favourable to long-lived travelling disturbances, because of the thin layer of moist air overlaid by subsiding dry air. Rainfall in these regions may therefore predominantly result from convection associated with daytime heating, hence the larger W3 values.

A similar agreement between the two data sets is found for the mean diurnal phase (Figure 3), though TMPA fields are less smooth than those of PERSIANN. Whatever the season, a late afternoon maximum (15:00 UTC, i.e., the 3-h time-slot starting at about 15:30–17:00 LST) dominates over most land areas, as a result of daytime heating. It contrasts with the eastern Atlantic Ocean where the maximum is in the morning (mainly 06:00–09:00 UTC). However, several areas show shifts in the maximum, especially in TMPA. These shifts generally materialize as gradual delays from east to west, but the apparent propagation is much slower than the diurnal course of the sun. For instance, in January, northeast of

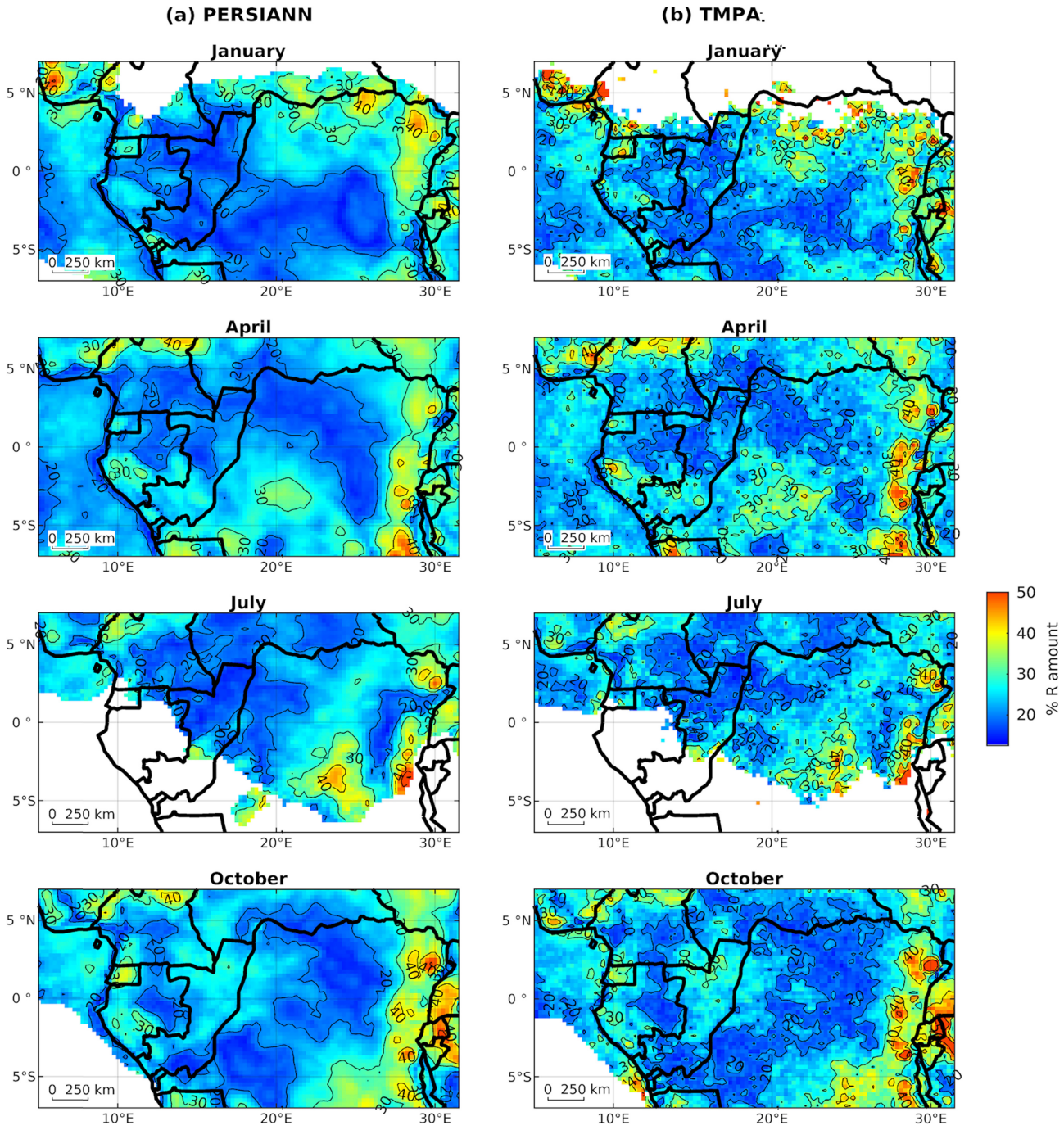

FIGURE 2 Rainfall of the mean wettest 3-hourly time-slot (W3) as a percentage of mean daily rainfall, based on PERSIANN (left panels) and TMPA data (right panels) for January, April, July and October. The percentage may theoretically vary between 12.5% (= constant rainfall across all the eight 3-h time slots in a day) and 100% (= a single 3-h period is wet). Areas with a mean monthly rainfall below 20 mm are masked.

the bend of the Congo River (25° E, 2° N), the maximum shifts from 15:00 to the evening and the night as one moves to the southwest, with the peak being as late as early morning (03:00 to 06:00) near 17° E, 3° S. Other cases of east to west phase shifts are found in April north of the Congo River (3° N, 19–30° E), in July over the Cuvette Centrale (0° N, 15–25° E), in October in Kasai (5° S, 16–25° E). Conspicuously, the shift displays a meridional component which changes seasonally: in January the phase shift of the diurnal maximum is clearly from northeast to southwest, in July from southeast to northwest, while in April and October the phase propagates more zonally. Over the Atlantic Ocean, an apparent westward-propagation of the rainfall phase is also

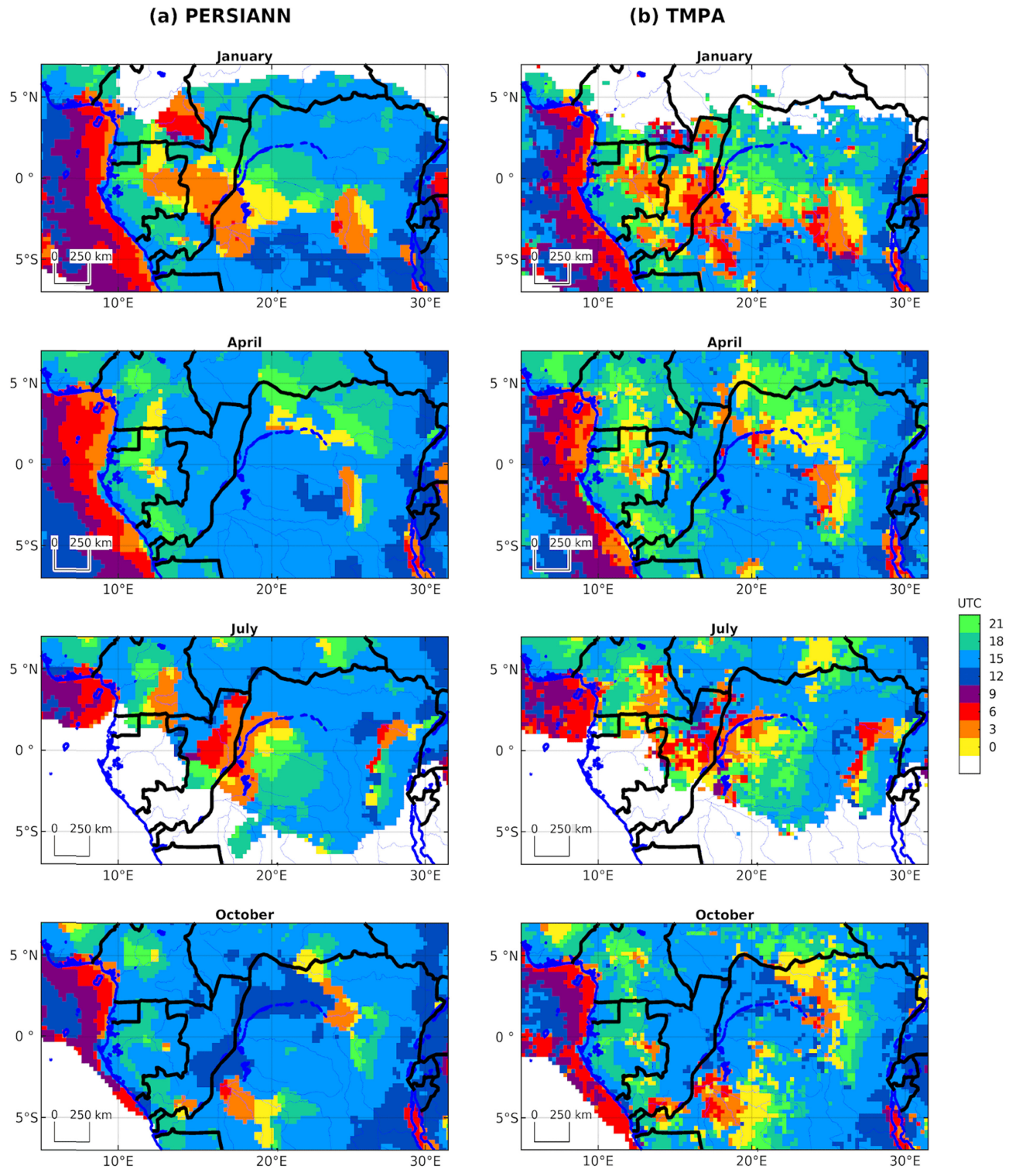

FIGURE 3 Phase of the mean wettest 3-h period, based on PERSIANN (left panels) and TMPA data (right panels) for January, April, July and October. Areas with a mean monthly rainfall below 20 mm are masked. All timings are UTC and correspond to the start of the 3-h time-slot. Local time is UTC + 1 at 15° E and UTC + 2 at 30° E.

noticeable throughout the year, with an early peak (03:00 to 06:00) near the coast gradually shifting to 12:00–15:00 further west. The patterns are less clear in the Western part of Central Africa (10–16° E) although propagations in the opposite direction are noticeable (from 15:00 near the coastline to 18:00–24:00 further east), especially in April and July in Cameroon, suggesting a role of sea breezes.

The above phase maps sometimes mask out more complex diurnal distributions. Many parts of Central Africa show a secondary maximum in their diurnal rainfall cycle, especially at night (00:00–03:00) over much of the Western Cuvette Centrale (15–20° E). Over the core part of the region (12–30° E, 5° S–5° N), when taking all months together, 45% of the grid-points (TMPA data) show a 15:00 main rainfall maximum (Figure 4). However, a secondary maximum is found over more than 20% of the grid-points for each 3-h slot from 00:00 to 06:00. Overall, nighttime rainfall (21:00 to 03:00 time-slots) generally accounts for 30%–50% of the total rainfall. Jackson et al. (2009) also noted a substantial MCS activity at night, especially in the central Congo Basin. Nicholson (2022) noted that this nighttime rainfall peak is much less common in Amazonia than in Central Africa. In the Sahel, while a vast majority of nocturnal rainfall occurrence is associated with the propagation of MCSs developed in the afternoon, cases of nighttime MCSs exist which are still poorly understood but partly dependent on the Intertropical Front location (Vizy & Cook, 2018). In Central Africa, the movement of rain cells developed in the afternoon cannot solely account for this maximum, because Figure 4 does show a distinct secondary peak at night. Samba-Kimbata (1988) suggests that it could result from a reactivation of stratiform clouds by nighttime radiative cooling. The same process is proposed for Amazonia by Lin et al. (2000). Over the same region, Negri et al. (2002) added that land-river circulations could account for the lower afternoon and higher nocturnal rain rates along major rivers. This hypothesis may hold for parts of the Congo Basin featuring large waterways. As suggested in other cases of nocturnal maxima for South America (Junquas et al., 2018) and the Himalayan foothills (Sugimoto et al., 2021), the role of downslope circulations west of the Western Rift Highlands cannot be ruled out.

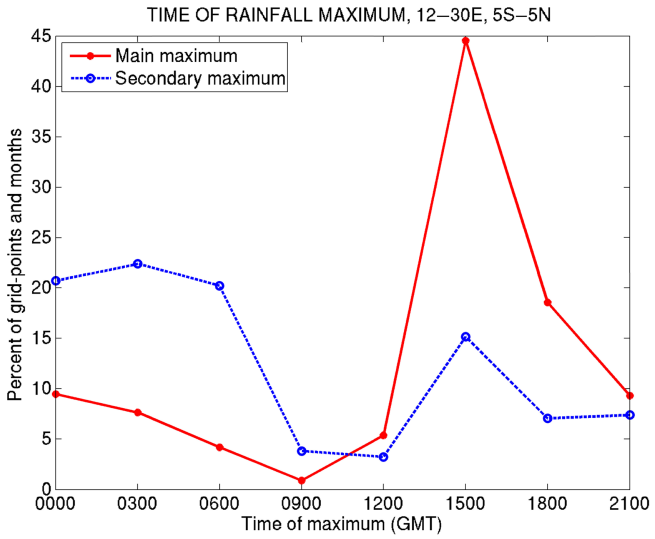

FIGURE 4 Diurnal phase of the rains (TMPA data, monthly time-scale) expressed as the percentage of grid-points, over the region 12–30° E, 5° S–5° N, which display a peak in each 3-hourly time-slot. Red line: main rainfall maximum; dashed blue line: secondary maximum. A secondary maximum is defined for bimodal diurnal regimes as a second main local peak (i.e., 3-h rainfall higher than both the previous and the following 3-h time-slots).

TMPA time-longitude plots of the mean diurnal cycle near the equator (1° S–0° N, Figure 5) well show the apparent propagations found for some longitudes and seasons. This is the case over the ocean (west of 10° E) where a westward shift of the local precipitation maximum occurs from 00:00 to 12:00 in January and April, while in July the sea-surface temperature south of the equator remains too low to drive local convection, inducing only low-level rainless clouds (Champagne et al., 2023; Dommo et al., 2018; Moron, Camberlin, et al., 2023). Over the continent, the most obvious and recurrent propagation is found west of the Mitumba Mountains near 29° E from the early afternoon (12:00) to the late night. The propagation can be traced down in the main precipitation maximum over a distance of about 500 km from 29° E to 24–25° E, except in July where it is slower (Figure 5). In the central Congo Basin (15–25° E), there is only limited evidence of propagative features in April and October, with an unambiguous 15:00 rainfall peak, but in July and January westward propagation is more obvious between 15:00 (25° E) and 06:00 (17° E). More complex diurnal phase variations are found in the west around the Bateke Plateaux (13–15° E), Chaillu Mountains (11–12° E) and coastal plains, where an evening rainfall maximum (18:00–21:00) is suggested to result from both a westward shift of afternoon cells and an eastward propagation of the sea breeze (9–11° E).

In summary, the late afternoon convective maximum is overwhelming, but there is often a delay of the peak rainfall from the main genesis areas towards the evening hours, possibly denoting the shifts of convective systems. Additionally, there is a frequent nighttime maximum, whose occurrence is hypothesized to be related either to the shift of rainfall disturbances, a reactivation of stratiform clouds through nocturnal cooling, sea/river-land breezes or dynamical convergence related to katabatic flows, near mountain slopes. Substantial seasonal alterations are found to the diurnal rainfall distribution patterns.

4.2 | Rain cells development and propagation

The lifecycle of individual rain systems is now examined using 1-h PERSIANN rainfall estimates as the 3-h

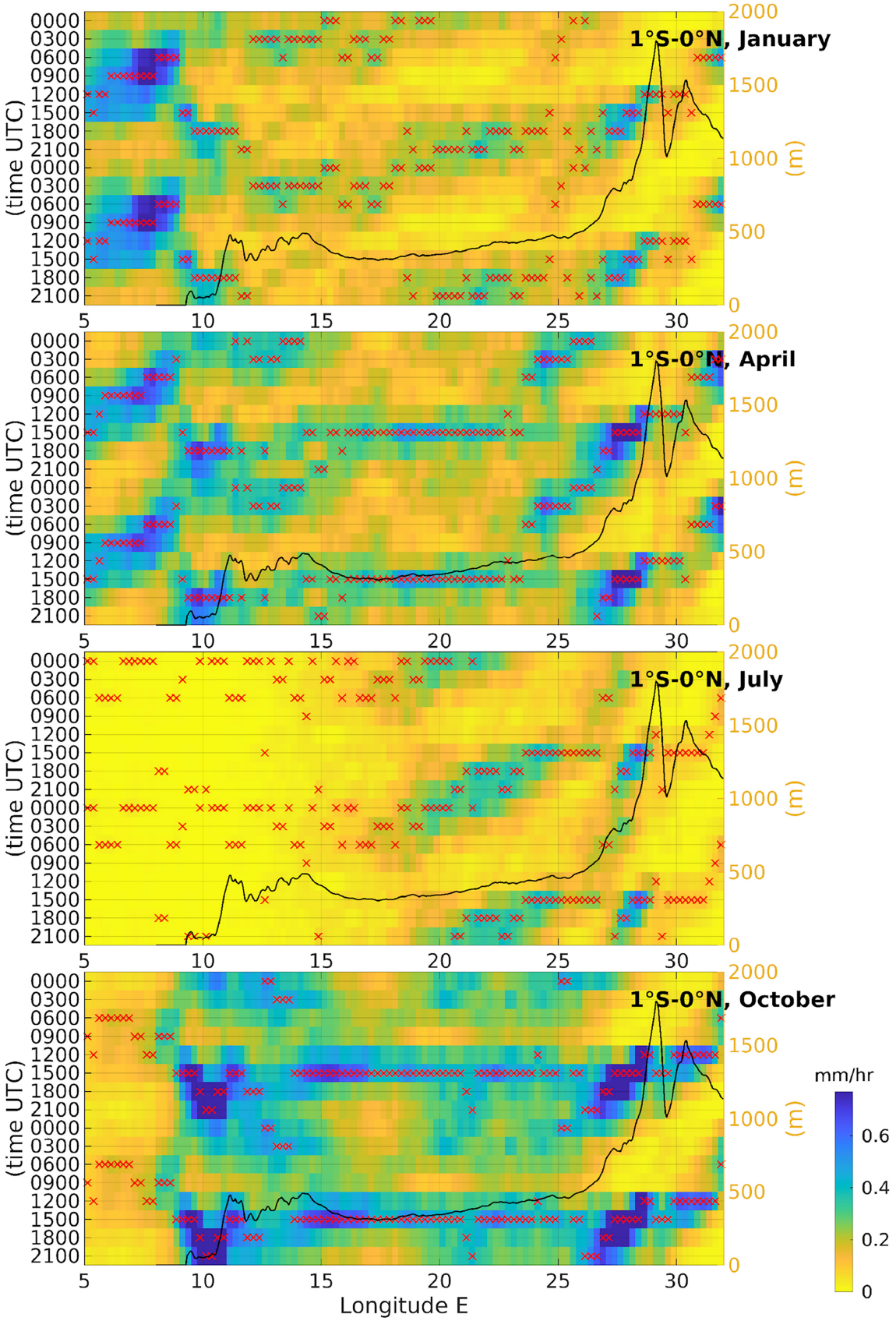

FIGURE 5 Time-longitude plots of TMPA mean diurnal rainfall variations for selected months along the equator (1° S–0°). For clarity, two diurnal cycles are plotted. Red crosses indicate the time-slot of maximum precipitation at each longitude. The black line shows the elevation (right axis).

TABLE 1 Statistics of rain cells over Central Africa as detected from 2001 to 2017 PERSIANN data.

		Mobile rain cells					
	Stationary rain cells	All	Eastward-moving	Westward-moving	Eastward-moving ≥6 h	Westward-moving ≥6 h	Duration ≥24 h
Mean number per year	917	2466	351	2115	113	733	30
Percentage (bracketed: among mobile raincells)	27.1	72.9	(14.2)	(85.8)	(4.6)	(29.7)	(1.2)
Average speed ($m \cdot s^{-1}$)	/	6.7	5.6	6.9	7.1	9.3	11.2
Duration (h)	1.05	5.6	5.5	5.8	10.7	10.7	29.4
Mean rainfall intensity ($mm \cdot h^{-1}$)	4.3	4.8	4.7	4.9	5.2	5.3	5.8
Peak genesis time (UTC)	1500	1400	1400	1400	1200	1300	1200
Average maximum area during lifetime (10^3 km^2)	3.9	33.0	31.8	33.3	68.2	67.0	163.0

resolution of TMPA is too coarse. For 2001–2017, 57,531 rain cells were detected, that is, 9.3 rain cells per day. Out of these, 6.8 rain cells per day were mobile (defined as showing a shift in their centre of gravity during their lifetime), that is, 72.9% (Table 1). Stationary rain cells are still quite numerous, but overwhelmingly of small size (89% do not exceed 8000 km^2, while 80% of the mobile rain cells are over 8000 km^2), and they quickly decay (99.1% of stationary rain cells have a 1-h lifetime).

Figure 6 shows the spatial patterns of rain cells initiation and dissipation, based on the location of their centre of gravity, for all rain cells (mobile and stationary). The patterns for mobile cells only (not shown) strongly correlate to those of Figure 6 ($r = 0.99$ and 0.96 for the initiation and the dissipation, respectively). A prominent area of initiation stands out near the north–south oriented highlands west of the Rift Valley, in the east of the Congo Basin. The peak is located near 28° E–2° S, in the Mitumba Mountains, not on the mountain tops or ridges but west of them (about 80–120 km away, at elevations near or below 1000 m), that is, in the lee of the prevailing mid-tropospheric easterly flow. This feature has also been noted by Hartman (2021). Another distinct area of frequent initiation is in the northwestern corner of the region, slightly west of the Cameroon Highlands (9.5° E, 6.5° N). Elsewhere, initiation is more evenly distributed. However, minor relief and hydrographical features still have an influence. Rain cells more often initiate over interfluves (like in the Cuvette Centrale near 22.5° E, 0.5° N—Figure 6a) while major river courses, being cooler surfaces at daytime, generally show lower frequencies. At the border between Gabon and Congo-Brazzaville, the Batéké Plateau (Figure 1), although not particularly high, is a local prominent area of rain cell generation.

Spatial patterns of dissipation (Figure 6b) bear similarities with those of initiation (pattern correlation: 0.78 for $n = 5220$ grid-points). This is due to the brief lifetime of many rain cells (46.5% do not exceed 2 h). However, peaks of dissipation frequencies are generally shifted to the west (e.g., $r = 0.85$ with the initiation map shifted westward by 0.25° longitude), which points to a dominant westward propagation of the cells. Additionally, the dissipation map is smoother than that of initiation because of both the spread of rain cells in different directions, as a result of different synoptic-scale airflows, and the uneven lifetime of the rain cells.

Table 1 provides additional statistics on mobile rain cells. Their average duration is 5.6 h (about 1 h for stationary ones), with minor seasonal changes (Figure 7a). This matches the most probable lifetime of Central Africa MCSs (6 h) obtained by Nguyen and Duvel (2008). Mobile cells developed from February to April tend to last slightly longer (5.9–6.2 h) than in other months. Long-lived disturbances account for a small percentage of all rain cells: only 1.2% of mobile cells have a lifetime of at least 24 h (i.e., about 30 systems every year). This may be a slight underestimation because some disturbances travel out of the study region and their full lifetime is therefore not accounted for.

The average propagation speed is 6.7 $m \cdot s^{-1}$. This is much lower than the ranges provided in previous studies of Central Africa MCSs (12–20 $m \cdot s^{-1}$ in Nguyen & Duvel, 2008; 8–16 $m \cdot s^{-1}$ in Laing et al., 2011; more than 9 $m \cdot s^{-1}$ over land areas in Hartman, 2021). However, maps published by Lafore (2017) show that in July–September Central Africa MCSs have a lower propagation speed than those of the Sudano-Sahelian belt. Importantly, mobile systems which have a longer lifetime tend to show a faster movement (Table 1). The mean speed of

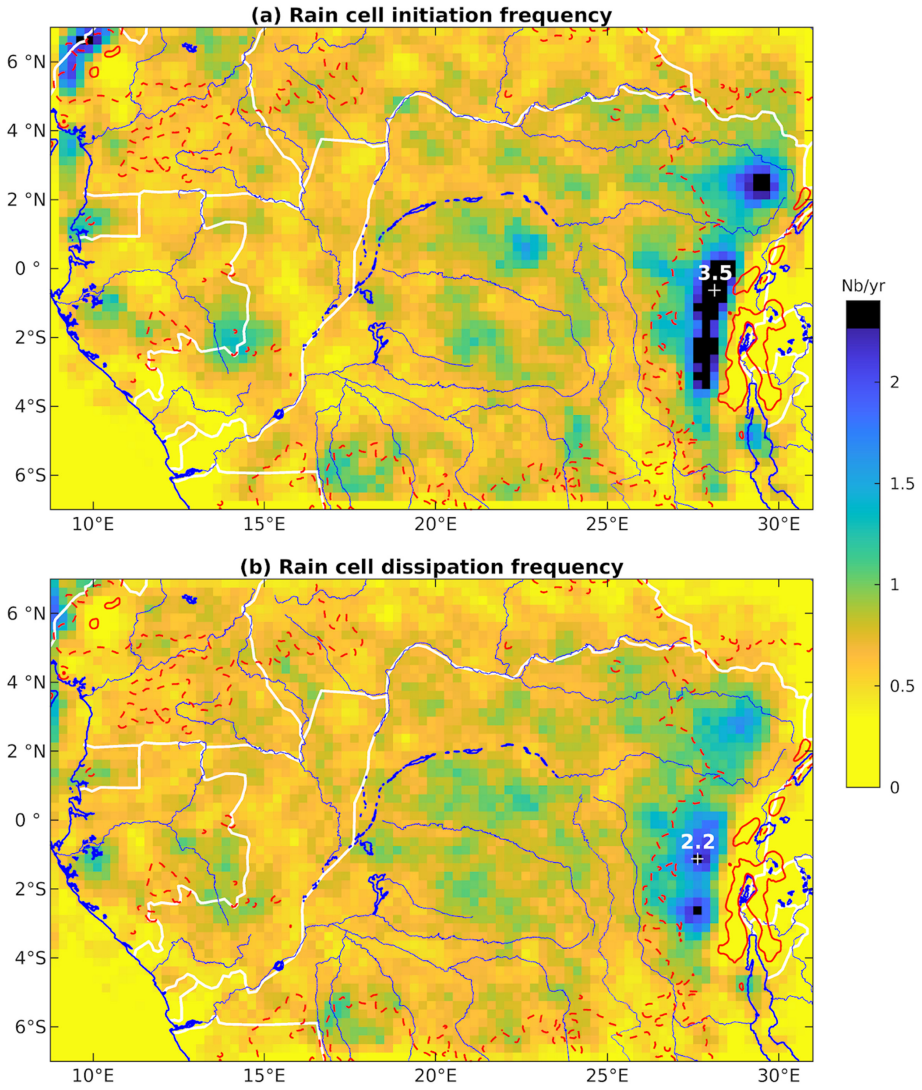

FIGURE 6 Mean annual frequency of rain cells initiation (top) and dissipation (bottom) in each 0.25° grid cell, based on the centre of gravity of each rain cell. Both mobile and stationary rain cells are included. White crosses indicate peak values. Thin red lines show 650 m (dashed) and 1800 m (solid) elevation contours.

mobile systems lasting less than 6 h (5.5 $m \cdot s^{-1}$) is half that of the systems whose lifetime reaches 24 h (11.2 $m \cdot s^{-1}$). This explains the apparent discrepancy in the average propagation speeds between this study and the previous ones which considered large-scale convective systems only. The propagation speed undergoes very little seasonal variations (Figure 7b). However, stationary systems are slightly less frequent in January–April (about 25% of all systems, Figure 7b) than during the rest of the year (27%–30%), in agreement with mean rain cell durations. As mentioned above, almost all of these stationary systems are very short-lived and small (on average 3900 km^2, against 33,000 km^2 for mobile systems at their maximum size, Table 1).

As expected, the longer-lasting systems additionally tend to be bigger (Table 1): those which last at least 6 h have an average maximum size of 67,100 km^2 and 163,000 km^2 for those which last at least 24 h. The maximum size reached across the lifecycle of mobile cells is actually strongly correlated to the duration of the cells ($r = 0.67$ for 57,531 events). The average rainfall intensity is also positively correlated to the rain cell size ($r = 0.65$) and duration ($r = 0.66$). This is in broad agreement with Lochbihler et al. (2017), for the Netherlands, and with Liu (2011) and Fu et al. (2020), for the tropics as a whole, who found that the mean rain rate of rain cells generally increases with the increase of their area and duration. Different results have been obtained based on station observations in Bangladesh (Moron, Acharya, & Hassan, 2023) and Central Africa (Mengouna et al., 2024, personal communication), where the duration of storm events at a given site is uncorrelated to mean hourly intensities. This is not contradictory with the present study which considers rain cells along their entire lifetime, not point rainfall. The above-defined threshold (4 $mm \cdot h^{-1}$) also excludes light rains which often take a great part of the duration of a given storm when observed from a fixed location. A last reason for the discrepancy could be that biases in the satellite rainfall estimates depend on the size of the rain cells. Large-scale systems

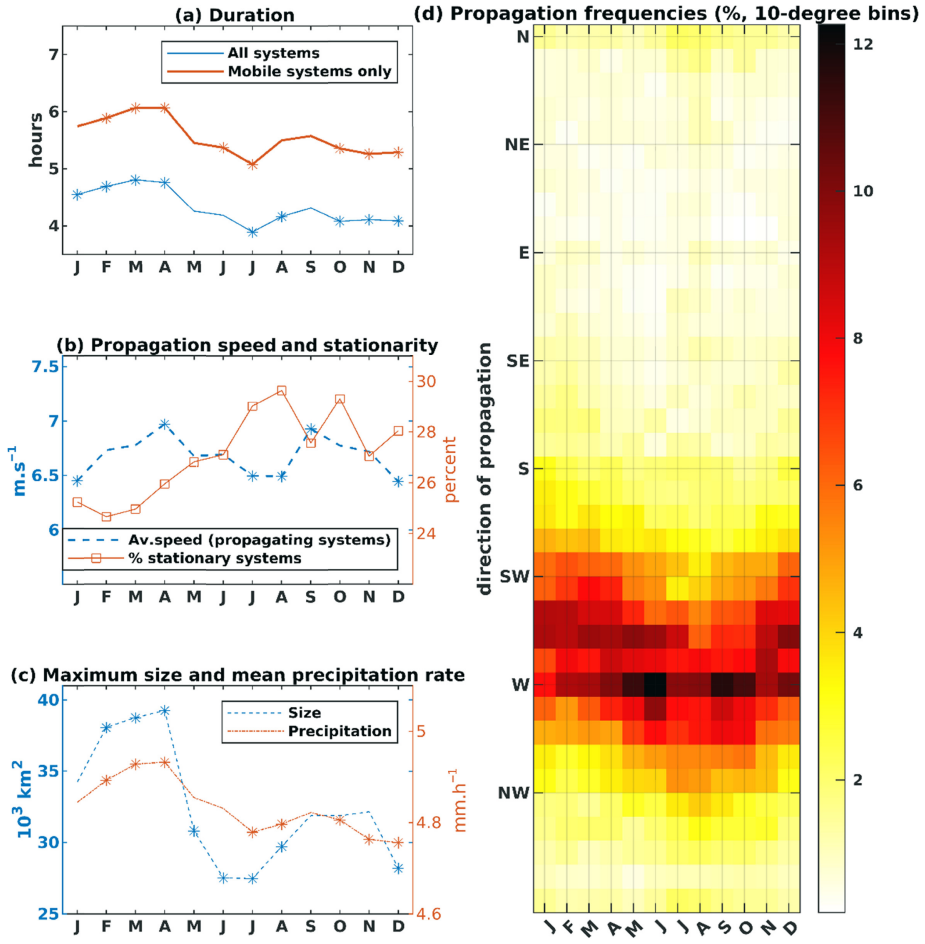

FIGURE 7 Average monthly duration (a), propagation speed (b), maximum size and mean precipitation rate (c) and propagation direction (d) of rain cells. Panel (b) also shows the percentage of stationary rain cells. In panels (a), (b) and (c) stars denote months where the statistics are significantly different from the annual mean (*t*-test, $p < 0.05$).

characterized by low infrared brightness temperature include large anvil clouds with little precipitation, which could positively bias the size-intensity relationship. Note however that in Central Africa the variations in the cells rainfall intensity are modest, since most cells (97%) do not exceed 6 mm·h^{-1}. This means that the total rainfall amount brought by a cell depends much more on its lifetime and size than on its intensity, though (contrary to the Eulerian view based on storm rainfall at a given site) the three parameters are interrelated.

Seasonal patterns of rain cell properties show quite large variations in cell sizes (Figure 7c). While the maximum size is, as expected, lower in the drier months (especially in December and June–July), there is a marked asymmetry between the two rainy seasons. Rain cells are much larger in February–April (about 39,000 km^2) than in September–November (about 32,000 km^2). This more or less reflects the seasonal cycle of rain cells' duration (Figure 7a). By contrast, the variations in precipitation intensity per rain cell (Figure 7c, line with squares) are small, but somewhat related to cell sizes.

In the zonal direction, an overwhelming majority (86%) of the mobile rain cells propagate westward and only 14% eastward (Table 1). This is consistent with Laing et al. (2011) and Nguyen and Duvel (2008), and is related to the dominant mid- and upper-tropospheric easterly flow. However, the seasonal cycle displays conspicuous shifts in the meridional component of the propagation (Figure 7d), which have not been documented before. From November to April, most systems show a southward component in their westward displacement, while in the rest of the year the meridional component is closer to zero or slightly northward. This agrees with Laing et al. (2008) who found, though over a domain more to the north, that the general movement of cold cloud systems is slightly south of west. This issue of meridional propagation will be further discussed below. There is little difference between westward- and eastward-propagating systems in terms of duration and size (westward propagating systems being marginally longer-lasting and bigger). However, an interesting feature is the higher propagating speed of westward-moving systems (Table 1). This again likely results from the dominant easterly mid-tropospheric winds.

The diurnal cycle of the rain cell genesis time peaks at 15:00 UTC for stationary systems, at 14:00 for mobile systems (for both eastward and westward propagating

systems, Table 1). Genesis frequencies then gradually decrease in the night, reaching a minimum in the morning. Note that the systems which have a long lifetime (≥6 or 24 h) initiate a little earlier (12:00 or 13:00, Table 1). Though a large number of rain cells are initiated west of the mountain ridges near 28° E, this does not bias the statistics. The afternoon peak in rain cells initiation is almost ubiquitous, though a secondary peak is also found in the early night in the western part of the region (not shown). As noted above, statistics on rain cells timings are almost unbiased with respect to LST, since there is only a 1.3 h LST lag between the easternmost and westernmost parts of the region. Dissipation times for mobile systems peak at 16:00 UTC (not shown), with a still very high and almost flat rate until 19:00, after which a drop occurs. Dissipation frequencies are then almost constant during the night.

4.3 | Comparison between wind flow and motion of rain cells

Time-height diagrams of the mean monthly zonal and meridional components of the wind over Central Africa (7° S–7° N, 9–31° E) are plotted (Figure 8). Zonal winds show the characteristic monsoon westerlies below about 850 hPa (strongest in August), overlaid by easterlies. The mid-tropospheric (600–650 hPa) African Easterly Jets (AEJ) are best developed during the rainy seasons (March–April, October–November) (Kuete et al., 2020; Nicholson & Grist, 2003). Upper tropospheric easterlies (Tropical Easterly Jet) strengthen in boreal summer (July–August).

Whereas zonal winds show constant direction whatever the season (westerlies below about 850 hPa, easterlies above) and a bimodal seasonal distribution for speeds, in the meridional direction the pattern is very different, with a seasonal reversal reflecting the shifts in the Hadley circulation and ITCZ/rainbelt location across Africa. Mid-tropospheric (700–600 hPa) northerlies in boreal winter give way to southerlies in boreal summer. An opposite pattern is found in the upper troposphere (southerlies in boreal winter, northerlies in summer). This reflects, in broad terms, the influence of the northern Hadley cell in boreal winter and of the southern Hadley cell in boreal summer. These are relatively well-known features of the atmospheric circulation over Central Africa (e.g., Dezfuli, 2017; Longandjo & Rouault, 2020; Neupane, 2016), although most of the studies focus on the zonal component of the circulation rather than the meridional component. A hitherto unnoticed feature is the gradual elevation shift of the shear line between northerlies and southerlies from January (near 900 hPa) to August (near 600 hPa), denoting a progressive thickening of the monsoon circulation towards the boreal summer.

As both the mean meridional component of the wind and the mean meridional component of rain cells propagation show seasonal changes, the two variables are plotted together on a monthly basis (Figure 9). We consider the 650 hPa level near the AEJ core and where a shift occurs between northerlies and southerlies across the year (Figure 8). The wind is averaged over the whole domain (7° S–7° N, 9–31° E). Figure 9 shows that besides the general westward motion of air and rain cells, there is also a strong similarity in the seasonal changes of the meridional components. Southward motion is best evidenced in December–April, the boreal winter, and especially from January to March, for both air and rain cell movements, while the strongest northward motion occurs over a shorter period in the austral winter (July–September, with a maximum in August) for both variables. The meridional component is however larger for wind than for rain cells. Both the winds and the rain cell

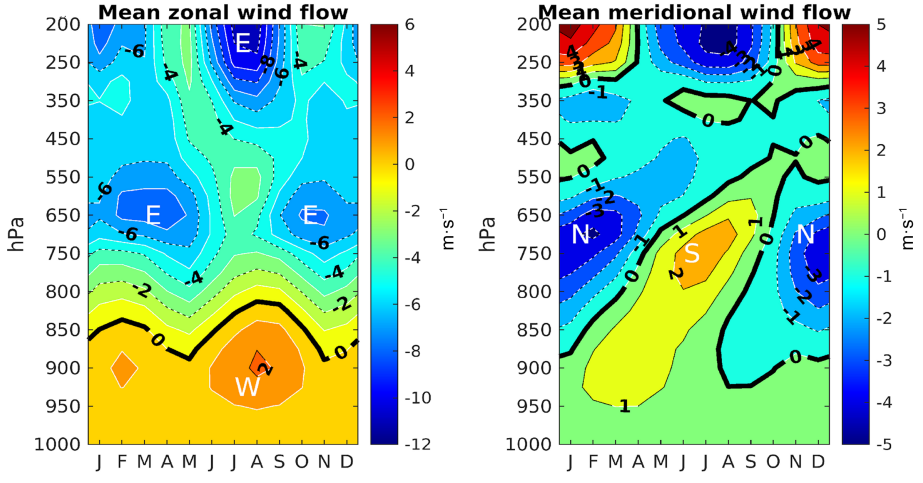

FIGURE 8 Seasonal cycle of mean zonal and meridional winds over Central Africa (7° S–7° N, 9–31° E) as a function of pressure levels (ERA5 reanalysis).

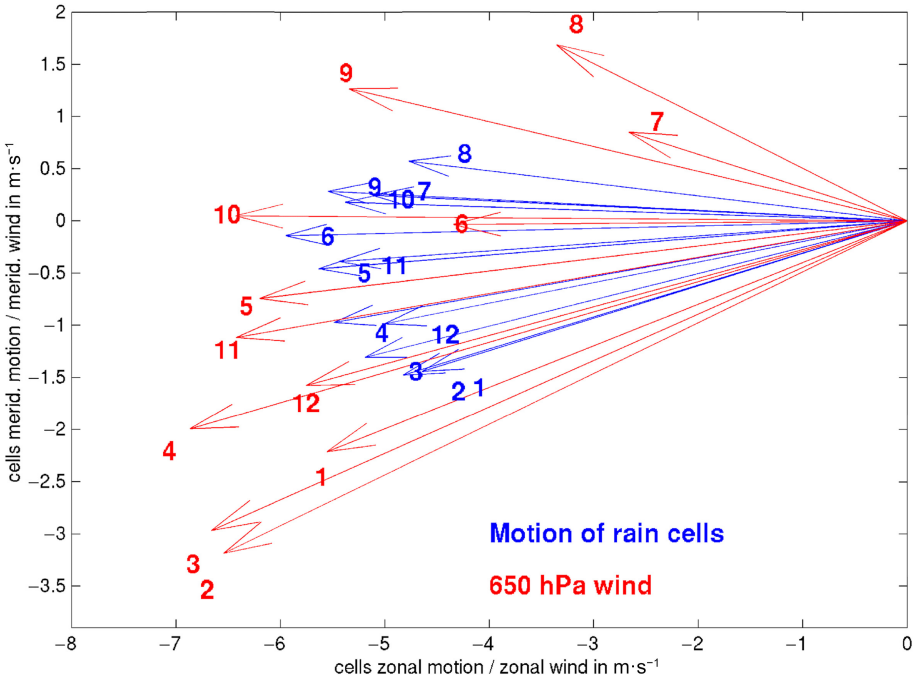

FIGURE 9 Mean motion of rain cells over Central Africa as a function of the months (1 = January, 2 = February, etc...), and 650 hPa mean wind flow (7° S–7° N, 9–31° E), in $m \cdot s^{-1}$.

propagations are almost zonal in June and October. The correlation between the mean monthly values of the rain cells' meridional propagation and of the meridional component of the wind is 0.98. Rain cells' annually averaged propagation speeds are slightly lower than wind speeds (6 $m \cdot s^{-1}$ as against 6.4 $m \cdot s^{-1}$). The exception is from June to August when rain cells propagate faster than the average 650 hPa wind speeds. This is when mid-tropospheric easterlies are weakest (Figure 8). Jeandidier and Rainteau (1957) and Tschirhart (1959) noted that squall lines over Central Africa were travelling faster than the prevailing mid-tropospheric easterly winds, but our study shows that this holds only for the longest-lived rain cells (also the largest). When including smaller size rain cells the agreement with the wind speed is better.

A closer examination is now carried out by considering each tropospheric level between 200 and 1000 hPa, and individual rain systems. The wind direction is again averaged over 7° S–7° N, 9–31° E, but now taken on the day of the rain cell itself, more precisely in the middle of each cell's lifetime. Figure 10 plots the frequency of the minimum angle between rain cells motion vectors and wind vectors, considering all the pressure levels selected (panel a), and the pressure level at which this angle is smallest (panel b). Most of the time, the angle is small, not exceeding 21° for almost 80% of the disturbances, and 3° for 38% of them. Although there is quite a large spectrum of levels at which the minimum angle is recorded, the best coincidence is obtained at 700 hPa, and the least one below 900 hPa. This confirms that mid-tropospheric wind flows are instrumental in the displacement of the rain cells. It is nearly independent of the rain cells scale and origin, thus not restricted to MCSs as in Hartman (2021) who noted that the westward displacement of Central Africa MCSs, in the rainy seasons, matched the 650 hPa wind field.

Correlations between the zonal (U) and meridional (V) components of the wind and those of the rain cells motion are next plotted on Figure 11. Since there are seasonal variations in the rain cells' locations, instead of averaging winds over the whole study region as above, we now consider winds at the cell's centre of gravity across its entire lifetime, that is, using collocated data for winds and rain cells movement. Figure 11a first displays the correlations between the mean annual cycles of winds and rain cells motions. The motions for any given month are computed as an average over all individual cells observed in this month. For V, two highly significant peaks ($p < 0.001$) appear at 650 hPa ($r = 0.98$, consistent with the value obtained above) and at 400 hPa (0.92). This confirms that the seasonal changes in the mean meridional propagation of rain cells strongly follow those of mid-tropospheric winds. A strong negative correlation, out-of-phase with that of the mid-tropospheric winds, is found in the lower troposphere ($r < -0.90$), which will be discussed below. Correlations with U are non-significant at $p = 0.05$ and much weaker than with V, suggesting that the weaker June–August mid-tropospheric easterlies do not induce any reduction in the westward propagation speed of the cells, as also shown on Figure 9.

When considering the 41,917 individual mobile rain cells (Figure 11b), correlations are much lower due to the noise contained in the data at this time-scale, but for V

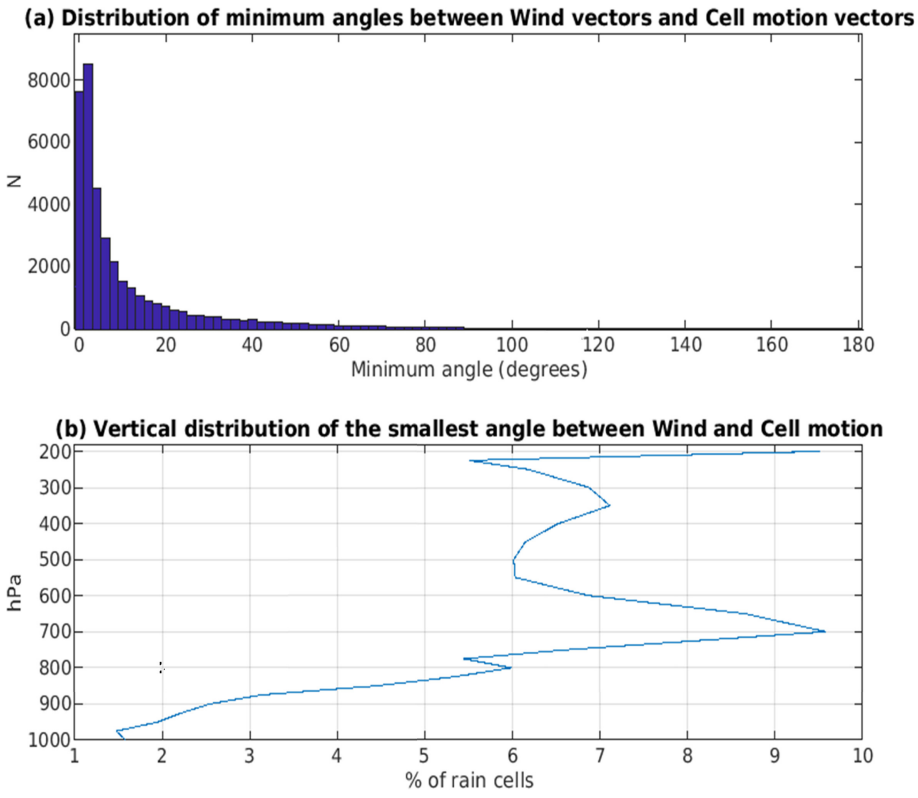

FIGURE 10 (a) Frequency distribution of the minimum angle between the motion vector of individual rain cells and the wind vectors between 1000 and 200 hPa (taken in the middle of each cell's lifetime); (b) Pressure level at which is found the smallest angle between the wind vectors and the cells motion vectors (only for rain cells showing a minimum angle of less than 20° with wind), expressed as a percentage of all rain cells.

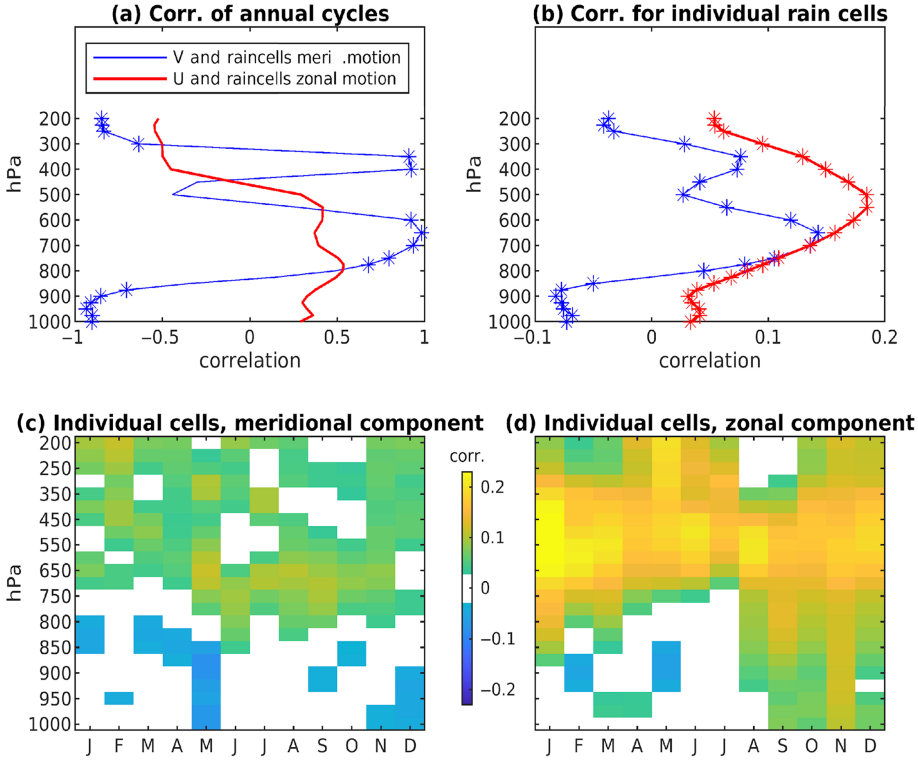

FIGURE 11 Correlations between the wind flow at different pressure levels and the motion of rain cells, based on their centre of gravity: meridional wind with meridional motion of the cells (thin blue line), zonal wind and zonal motion of the cells (thick red line), for the mean annual cycle (a) and for individual rain cells (b). In (c) and (d), the correlations for individual rain cells are plotted separately for each month (meridional wind and meridional motion in (c), zonal wind and zonal motion in d). Stars in (a) and (b) show statistically significant values ($p < 0.05$) while in (c) and (d) nonsignificant values ($p > 0.05$) are masked.

the mid-tropospheric (650 hPa) positive correlation peak is still obvious (0.14, significant at $p < 0.001$). This agrees with the above finding that southward (northward) air motion around this level accompanies southward (northward) rain cell propagation. Negative correlations with V are found in the lower troposphere. For U, based on individual rain cells, positive correlations (0.18) are found near 500–600 hPa (Figure 11b), suggesting that stronger easterlies at this level may be related to an enhanced westward movement of the rain cells.

The correlations found in Figure 11b may be influenced by the mean seasonal changes in winds and rain

cells motion. Hence, they are also plotted month by month to document the link between winds and individual rain cells (Figure 11c,d, for V and U respectively). Weak, positive correlations with V generally occur at 750 hPa and above. The 650 hPa level does not show prominently but it is near this level that the highest positive correlations are found from May to November. Correlations with U are stronger (especially in boreal winter), peaking around 0.20 near 400–600 hPa. On the whole, these results show that variations in mid tropospheric winds strongly control rain cell propagation, both in their mean seasonal variations (for their meridional component) and in the motion of individual rain cells (for their meridional and above all their zonal components). The monsoon flow (below 850 hPa, either V or U) does not display strong relationships with rain cells. This suggests that the negative correlation found when comparing the annual cycle of V at 900–1000 hPa and that of rain cells meridional motion (Figure 11a) is merely a covariation, the displacement of individual rain cells being almost independent from the lower tropospheric winds. This is corroborated by the fact that the correlations between the rain cells zonal motion and the vertical shear (U 650 hPa minus 925 hPa) are not higher than those obtained for mid-tropospheric zonal winds (not shown). These results are valid at the scale of Central Africa as a whole and do not exclude a possible role of low-level winds in some regions, like near the Atlantic Ocean, where the more complex diurnal regimes suggest a greater variety in the rain cells' displacements.

5 | CONCLUSION

An analysis of diurnal rainfall distribution and rain cell motion over Central Africa was carried out which, contrary to most previous studies, considered all wet patches rather than mesoscale systems only, and used precipitation estimates instead of brightness temperature, therefore enabling to derive useful statistics in terms of rainfall characteristics. Based on TMPA and PERSIANN 3-hourly rainfall estimates, over land areas the dominant afternoon maximum described by Jackson et al. (2009), Dezfuli (2017) and Vondou et al. (2017) is confirmed. However, the rainfall concentration in the peak 3-h period is moderate (20%–30%) in a large part of the region (except near mountain ranges). Substantial rainfall occurs at night. This includes a secondary maximum at over 20% of the grid-points for each 3-h slot from 00:00 to 06:00 UTC. Seasonal changes in the diurnal rainfall distribution are also found. For instance, the afternoon peak is more prevalent in April than in January, where across the central part of the region the peak is progressively delayed, suggesting a greater role of travelling disturbances. Also noteworthy is the seasonal change in the meridional propagation of the peak diurnal rainfall, southwestward in January, and northwestward in July.

These characteristics of diurnal rainfall variations were compared with data on rain cells motion. To that end, intense rain cells (4 $mm \cdot h^{-1}$ threshold) were tracked using PERSIANN hourly data. The peak genesis time of the rain cells is slightly ahead the diurnal phase of the rains. Stationary systems develop somewhat later (15:00 UTC) than mobile ones, especially long-lasting systems (12:00–13:00 UTC for those having a lifetime of at least 6 h). Consistent with Laing et al. (2011), the preferred initiation areas are slightly west of the high ground areas, the most prominent one being the meridional mountain ranges of eastern DRC.

There is a clear relationship between the size, duration and mean rainfall intensity of the rain cells, contrary to studies focused on storm properties at a given site, which found that mean intensity is uncorrelated to storm duration (Mengouna et al., 2024, personal communication; Moron, Acharya, & Hassan, 2023). The mean lifetime (5.6 h) agrees with the figures obtained for Central Africa MCSs (Nguyen & Duvel, 2008). However, the propagation speed (6.7 $m \cdot s^{-1}$) is much lower than in other studies (Laing et al., 2011; Nguyen & Duvel, 2008). This is because we include small size rain cells and not only MCSs. An important result is that the mobile systems which have a longer lifetime clearly move much faster. The lifetime and size of the rain cells display a semiannual cycle, with generally bigger and longer-lasting cells in the two rainy seasons, but there is an asymmetry between them. The boreal spring rains show larger and longer-lasting systems. By contrast, the boreal autumn season has a higher number of rain cells, including stationary ones, which contributes to explain why on average this season is wetter.

While most (86%) of the mobile rain cells propagate westward, the meridional component of the propagations is a distinctive feature of the rain cells characteristics. Contrary to other properties such as lifetime and propagation speed whose seasonal variations are small or show a semiannual pattern, the meridional component of the rain cells motion undergoes a well-defined annual cycle. A northerly component dominates in austral summer (peaking in January–February) and a weaker southerly component in boreal summer (peaking in August). This explains the tilted axis of propagation of the diurnal phase of the rains as noted above.

The average propagation speed of the rain cells is close to the mid-tropospheric (650 hPa) mean wind speed. The seasonal variations in the meridional wind flow match those of the rain cells propagation, with a southward direction in austral summer and a weaker northward direction in boreal summer. These changes also help to understand the seasonal variations of the

diurnal phase of the rains over Central Africa. The diurnal rainfall phase shifts correspond to the actual propagation of convective cells, where the daytime (afternoon) maximum is not prominent.

It is suggested that an appraisal of the variability in rain cells propagation and properties would help explain the intra-seasonal to seasonal rainfall variations over Central Africa, which remain poorly understood (Dezfuli, 2017; Pokam Mba et al., 2022). In view of the human-induced ongoing warming of the global atmosphere, which affects water vapour content and convective activity, we also recommend monitoring future changes in rain cell characteristics which are strong determinants of the local frequency and intensity of rain events.

AUTHOR CONTRIBUTIONS

Pierre Camberlin: Conceptualization; methodology; investigation; supervision; formal analysis; writing – original draft. **Vincent Moron:** Methodology; validation; writing – review and editing; conceptualization. **Nathalie Philippon:** Writing – review and editing; conceptualization; validation; methodology. **François Xavier Mengouna:** Writing – review and editing; conceptualization; validation. **Derbetini A. Vondou:** Writing – review and editing; conceptualization; validation.

FUNDING INFORMATION

This research was jointly funded by Institut National des Sciences de l'Univers, CNRS, France, and Centre National d'Etudes Spatiales (project WaTFor—Water and lighT availability in Tropical Forests), France.

DATA AVAILABILITY STATEMENT

Data sharing is not applicable to this article as no new data were created or analyzed in this study.

ORCID

Pierre Camberlin https://orcid.org/0000-0003-4896-2332

Derbetini A. Vondou https://orcid.org/0000-0002-8681-5328

REFERENCES

Andrews, P.C., Cook, K.H. & Vizy, E.K. (2024) Mesoscale convective systems in the Congo Basin: seasonality, regionality, and diurnal cycles. *Climate Dynamics*, 62(1), 609–630.

Baidu, M., Schwendike, J., Marsham, J.H. & Bain, C. (2022) Effects of vertical wind shear on intensities of mesoscale convective systems over West and Central Africa. *Atmospheric Science Letters*, 23(8), e1094.

Camberlin, P., Barraud, G., Bigot, S., Dewitte, O., Makanzu Imwangana, F., Maki Mateso, J.C. et al. (2019) Evaluation of remotely sensed rainfall products over Central Africa. *Quarterly Journal of the Royal Meteorological Society*, 145(722), 2115–2138.

Camberlin, P., Gitau, W., Planchon, O., Dubreuil, V., Funatsu, B.M. & Philippon, N. (2018) Major role of water bodies on diurnal precipitation regimes in Eastern Africa. *International Journal of Climatology*, 38(2), 613–629.

Capsoni, C., D'Amico, M. & Locatelli, P. (2008) Statistical properties of rain cells in the Padana Valley. *Journal of Atmospheric and Oceanic Technology*, 25(12), 2230–2244.

Champagne, O., Aellig, R., Fink, A.H., Philippon, N., Camberlin, P., Moron, V. et al. (2023) Climatology of low-level clouds over Western equatorial Africa based on ground observations and satellites. *Journal of Climate*, 36(13), 4289–4306.

Copernicus Climate Change Service (C3S). (2017) ERA5: fifth generation of ECMWF atmospheric reanalyses of the global climate. Retrieved March 5, 2020, from Copernicus Climate Change Service Climate Data Store (CDS) website: https://cds.climate.copernicus.eu/cdsapp#!/home

Dezfuli, A.K. (2017) Climate of western and central equatorial Africa. Oxford Research Encyclopedia of Climate Science, 66 pp. https://doi.org/10.1093/acrefore/9780190228620.013.511

Dommo, A., Philippon, N., Vondou, D.A., Sèze, G. & Eastman, R. (2018) The June–September low cloud cover in western Central Africa: mean spatial distribution and diurnal evolution, and associated atmospheric dynamics. *Journal of Climate*, 31(23), 9585–9603.

Fu, Y.F., Chen, Y.L., Zhang, X.D., Wang, Y., Li, R., Liu, Q. et al. (2020) Fundamental characteristics of tropical rain cell structures as measured by TRMM PR. *Journal of Meteorological Research*, 34(6), 1129–1150. Available from: https://doi.org/10.1007/s13351-020-0035-5

Gleixner, S., Demissie, T. & Diro, G.T. (2020) Did ERA5 improve temperature and precipitation reanalysis over East Africa? *Atmosphere*, 11(9), 996.

Hartman, A.T. (2021) Tracking mesoscale convective systems in central equatorial Africa. *International Journal of Climatology*, 41(1), 469–482.

Hong, Y., Hsu, K.L., Sorooshian, S. & Gao, X. (2004) Precipitation estimation from remotely sensed imagery using an artificial neural network cloud classification system. *Journal of Applied Meteorology*, 43(12), 1834–1853.

Howard, E. & Washington, R. (2019) Drylines in southern Africa: rediscovering The Congo air boundary. *Journal of Climate*, 32, 8223–8242. Available from: https://doi.org/10.1175/JCLI-D-19-0437.1

Huffman, G.J., Bolvin, D.T., Nelkin, E.J., Wolff, D.B., Adler, R.F., Gu, G. et al. (2007) The TRMM multisatellite precipitation analysis (TMPA): Quasi-global, multiyear, combined-sensor precipitation estimates at fine scales. *Journal of Hydrometeorology*, 8(1), 38–55.

Jackson, B., Nicholson, S.E. & Klotter, D. (2009) Mesoscale convective systems over western equatorial Africa and their relationship to large-scale circulation. *Monthly Weather Review*, 137, 1272–1294.

Jeandidier, G. & Rainteau, P. (1957) Prévision du temps sur le bassin du Congo - Monographies de la Météorologie Nationale (Paris). no. 9, 13 p.

Junquas, C., Takahashi, K., Condom, T., Espinoza, J.C., Chavez, S., Sicart, J.E. et al. (2018) Understanding the influence of orography on the precipitation diurnal cycle and the associated atmospheric processes in the central Andes. *Climate Dynamics*, 50, 3995–4017. Available from: https://doi.org/10.1007/s00382-017-3858-8

Kuete, G., Pokam, W.M. & Washington, R. (2020) African Easterly Jet South: control, maintenance mechanisms and link with Southern subtropical wave. *Climate Dynamics*, 54, 1539–1552. Available from: https://doi.org/10.1007/s00382-019-05072-W

Lafore, J.P. (2017) Deep convection. In: Parker, D.J. & Diop-Kane, M. (Eds.) *Meteorology of tropical West Africa: the forecasters' handbook*. Chichester, UK: John Wiley & Sons, pp. 161–223.

Lafore, J.P., Flamant, C., Guichard, F., Parker, D.J., Bouniol, D., Fink, A.H. et al. (2011) Progress in understanding of weather systems in West Africa. *Atmospheric Science Letters*, 12(1), 7–12.

Laing, A.G., Carbone, R.E. & Levizzani, V. (2011) Cycles and propagation of deep convection over equatorial Africa. *Monthly Weather Review*, 139(9), 2832–2853. Available from: https://doi.org/10.1175/2011MWR3500.1

Laing, A.G., Carbone, R.E., Levizzani, V. & Tuttle, J.D. (2008) The propagation and diurnal cycles of deep convection in northern tropical Africa. *Quarterly Journal of the Royal Meteorological Society*, 134, 93–109.

Lin, X., Randall, D.A. & Fowler, L. (2000) Diurnal variability of the hydrologic cycle and radiative fluxes: comparisons between observations and a GCM. *Journal of Climate*, 13, 4159–4179.

Liu, C. (2011) Rainfall contributions from precipitation systems with different sizes, convective intensities, and durations over the tropics and subtropics. *Journal of Hydrometeorology*, 12, 394–412. Available from: https://doi.org/10.1175/2010JHM1320.1

Lochbihler, K., Lenderink, G. & Siebesma, A.P. (2017) The spatial extent of rainfall events and its relation to precipitation scaling. *Geophysical Research Letters*, 44, 8629–8636. Available from: https://doi.org/10.1002/2017GL074857

Longandjo, G.N.T. & Rouault, M. (2020) On the structure of the regional-scale circulation over central Africa: seasonal evolution, variability, and mechanisms. *Journal of Climate*, 33(1), 145–162.

Moron, V., Acharya, N. & Hassan, S.Q. (2023) Storm types in Bangladesh: duration, intensity and area of intra-daily wet events. *International Journal of Climatology*, 43(2), 850–873.

Moron, V., Camberlin, P., Aellig, R., Champagne, O., Fink, A.H., Knippertz, P. et al. (2023) Diurnal to interannual variability of stratiform cloud cover over western equatorial Africa in May-October (1971-2019). *International Journal of Climatology*, 43 (13), 6038–6064. Available from: https://doi.org/10.1002/joc.8188

Moron, V. & Robertson, A.W. (2021) Relationships between subseasonal-to-seasonal predictability and spatial scales in tropical rainfall. *International Journal of Climatology*, 41, 5596–5624.

Negri, A.J., Xu, L. & Adler, R.F. (2002) A TRMM-calibrated infrared rainfall algorithm applied over Brazil. *Journal of Geophysical Research: Atmospheres*, 107(D20), LBA-15.

Neupane, N. (2016) The Congo basin zonal overturning circulation. *Advances in Atmospheric Sciences*, 33, 767–782.

Nguyen, H. & Duvel, J.P. (2008) Synoptic wave perturbations and convective systems over equatorial Africa. *Journal of Climate*, 21, 6372–6388.

Nguyen, P., Shearer, E.J., Tran, H., Ombadi, M., Hayatbini, N., Palacios, N. et al. (2019) The CHRS Data Portal, an easily accessible public repository for PERSIANN global satellite precipitation data. *Nature Scientific Data*, 6, 180296. Available from: https://doi.org/10.1038/sdata.2018.296

Nicholson, S.E. (2022) The rainfall and convective regime over equatorial Africa, with emphasis on The Congo Basin. In: Tshimanga R.M. et al. (Ed.) *Congo Basin hydrology, climate, and biogeochemistry: a foundation for the future*. Hoboken: John Wiley & Sons, pp. 25–48.

Nicholson, S.E. & Grist, J.P. (2003) The seasonal evolution of the atmospheric circulation over West Africa and equatorial Africa. *Journal of Climate*, 16(7), 1013–1030.

Parker, D.J. & Diop-Kane, M. (Eds.). (2017) *Meteorology of tropical West Africa: the forecasters' handbook*. Chichester, UK: John Wiley & Sons, p. 478.

Pokam Mba, W., Vondou, D.A. & Kamsu-Tamo, P.H. (2022) Central African climate: advances and gaps. In: Tshimanga R.M. et al. (Ed.) *Congo basin hydrology, climate, and biogeochemistry: a foundation for the future*. Hoboken: John Wiley & Sons, pp. 13–23.

Raghavendra, A., Zhou, L., Jiang, Y. & Hua, W. (2018) Increasing extent and intensity of thunderstorms observed over The Congo Basin from 1982 to 2016. *Atmospheric Research*, 213, 17–26.

Samba-Kimbata, M.J. (1988) Rythme diurne des précipitations dans le bassin forestier de la cuvette centrale d'Afrique. In: Pérard, J. & Escourrou, P. (Eds.) *Climats et Climatologie, Hommages au Pr Pagney*. Dijon: Centre de Recherches de Climatologie, pp. 431–438.

Sauvageot, H., Mesnard, F. & Tenorio, R.S. (1999) The relation between the area-average rain rate and the rain cell size distribution parameters. *Journal of the Atmospheric Sciences*, 56, 57–70.

Sugimoto, S., Ueno, K., Fujinami, H., Nasuno, T., Sato, T. & Takahashi, H.G. (2021) Cloud-resolving-model simulations of nocturnal precipitation over the Himalayan slopes and foothills. *Journal of Hydrometeorology*, 22, 3171–3188. Available from: https://doi.org/10.1175/JHM-D-21-0103.1

Taylor, C.M., Fink, A.H., Klein, C., Parker, D.J., Guichard, F., Harris, P.P. et al. (2018) Earlier seasonal onset of intense mesoscale convective systems in the Congo Basin since 1999. *Geophysical Research Letters*, 45, 13,458–13,467. Available from: https://doi.org/10.1029/2018GL080516

Tschirhart, G. (1959) *Les perturbations atmosphériques intéressant l'AEF méridionale*, Vol. 13. Paris: Monographies de la Météorologie Nationale, p. 32.

Vizy, E.K. & Cook, K.H. (2018) Mesoscale convective systems and nocturnal rainfall over the West African Sahel: role of the inter-tropical front. *Climate Dynamics*, 50, 587–614. Available from: https://doi.org/10.1007/s00382-017-3628-7

Vondou, D.A., Nzeukou, A., Lenouo, A. & Mkankam Kamga, F. (2010) Seasonal variations in the diurnal patterns of convection in Cameroon–Nigeria and their neighboring areas. *Atmospheric Science Letters*, 11(4), 290–300.

Vondou, D.A., Yepdo, Z.D., Steve, T.R., Alain, T.S. & Tchotchou, L. D. (2017) Diurnal cycle of rainfall over Central Africa simulated by RegCM. *Modeling Earth Systems and Environment*, 3(3), 1055–1064.

How to cite this article: Camberlin, P., Moron, V., Philippon, N., Mengouna, F. X., & Vondou, D. A. (2024). Seasonal variations in rain cells propagation over Central Africa and association with diurnal rainfall regimes. *International Journal of Climatology*, *44*(8), 2519–2536. https://doi.org/10.1002/joc.8466